Popular Benchmark Problems for Geometric Nonlinear Analysis of Shells

K.Y.Sze[1*], X.H.Liu[1#], S.H.Lo[2]

Departments of Mechanical[1] and Civil Engineering[2]

The University of Hong Kong, Pokfulam Road, Hong Kong SAR, P.R.CHINA.

ABSTRACT

In most, if not all, of the previous work on finite element formulation and nonlinear solution procedures, results of geometric nonlinear benchmark problems of shells are presented in the form of load-deflection curves. In this paper, eight sets of popularly employed benchmark problems are identified and their detailed reference solutions are obtained and tabulated. It is hoped that these solutions will form a convenient basis for subsequent comparison and that the tedious yet inaccurate task of reconstructing data points by graphical measurement of previously reported load-deflection curves can be avoided. Moreover, the relative convergent difficulty of the problems are revealed by the number of load increments and the total number of iterations required by an automatic load incrementation scheme for attaining the converged solutions under the maximum loads.

* corresponding author, email address : kysze@hku.hk

keywords : finite element, geometric nonlinear, benchmark, shell

on leave from *Department of Mechanics, Huazhong University of Science & Technology, Wuhan 430074, P.R.China.*

Published in *Finite Elements in Analysis & Design* **40**: 1551-1569 (2004).

1. INTRODUCTION

To examine or demonstrate the accuracy of new finite element models or the effectiveness of new nonlinear solution procedures, popular benchmark problems are often exercised and the predictions are compared to some reference solutions. Since analytical solutions of shell problems are very limited, most of reference solutions are previously reported numerical solutions. For linear benchmark problems, these solutions can be conveniently and concisely expressed in terms of numerical figures. To this end, the problem sets stipulated by MacNeal & Harder [1] and Hitchings, Kamoulakos & Davies [2] include some of the most widely attempted tests. Reference [1] has been well-received in the academic community. Reference [2] is a publication of UK's *National Agency for Finite Element Methods and Standards* (*NAFEMS*) and is mainly adopted by software developers for quality assurance. Noticeably, there are a number of cases common to both problem sets.

For geometric nonlinear analysis of shells, the most recent and relevant *NAFEMS* publication is probably the one by Prinja & Clegg [3]. Besides reference [3], more than forty research papers [4-49] on geometric nonlinear finite element formulation have also been surveyed. For conciseness, the reported predictions are mostly presented in the form of load-deflection curves. Occasionally, the results are reported numerically at a few selected load levels. In order to compare the predictions of new finite element models or procedures with their precedents, reconstructing the previously reported load-deflection curves by extracting data points using graphical measurement is the obvious and, perhaps, the only choice. The practice is not only inaccurate but also time consuming. In this context, eight sets of popular benchmark problems for geometric nonlinear analysis of shell are selected from those considered in references [3-49]. They are attempted by using ABAQUS's S4R four-node shell element models [50]. This paper will provide sufficient data points in numerical format so that the relevant load-deflection curves can be accurately and efficiently reconstructed. To reveal the relative convergent difficulty of the problems, the number of load increments and the total number of iterations required by ABAQUS's default automatic load incrementation scheme for attaining the converged solutions under the maximum loads are reported.

2. LOAD INCREMENTATION SCHEME

In the nonlinear solution procedure, the full Newton-Raphson method is used. The default convergence criteria are always employed and they are the simultaneous 0.5% force tolerance and 1% displacement tolerance. The default automatic load incrementation scheme in ABAQUS is adopted and the procedure is portrayed in Figure 1. Throughout the scheme, the maximum load P_{max}

will be automatically subdivided into NINC load increments which are not necessarily uniform. At the end of each load increment, a converged intermediate solution is obtained. This reduces the degree of nonlinearity from an intermediate solution state to another and enhances the chance of obtaining the ultimate solution. The latter is the one under the maximum load P_{max}. The scheme starts with the load increment ΔP set to the maximum load P_{max}. If the solution cannot converge within 16 iterations (counted by m) or if the solution diverges, the scheme abandons the increment and starts again with the load increment reduced to one-quarter of the previous value. If the solution still fails to converge, the scheme further reduces the increment size again. If the solution fails after 5 attempts (counted by n) of load increment reduction, the analysis will be stopped or aborted. On the other hand, it automatically increases the load increment by 50% if the last two converged solutions are both obtained within 5 iterations. If the scheme is not aborted, ABAQUS outputs NINC and NITER. The latter is the total number of iterations required to obtained the NINC converged intermediate solutions. In this paper, both NINC and NITER are reported to reveal the relative convergent difficulty of the considered problems.

For the sake of benchmarking, intermediate solutions given at uniform load intervals are desired. However, these solutions cannot be yielded by the afore-discussed default automatic load incrementation scheme. To this end, the solutions to be reported are computed by dividing the maximum load into a number of equal load increments NINC*, where further subdivision of the load increment is suppressed. In order that the ultimate solution can be successfully obtained, NINC* is often much larger than the NINC required by the default automatic load incrementation scheme.

3. BENCHMARK TESTS

In this section, eight sets of popularly employed geometric nonlinear benchmark problems on beams, plates, cylindrical shells and spherical shell are selected. A small portion of the considered structures are laminated. In the subsequent description, the following nomenclature is employed:

- ν: Poisson's ratio
- b: width
- E: elastic modulus
- G: shear modulus
- h: thickness of beam, plate or shell
- I: second moment of area
- L: length or longitudinal length
- M, M_{max} : applied moment and maximum applied moment, respectively
- NINC: the total number of load increments that yield the ultimate solution (determined by the default load incrementation scheme),

NINC*: the number of equal load increments used to obtain the plotted and tabulated data
NITER: the total number of iterations that lead to the NINC convergent solutions
P, P_{max} : applied force and maximum applied force, respectively
R: mean radius
U, V and W: displacements along the Cartesian coordinates X, Y and Z, respectively.

All benchmark problems to be presented have been attempted by ABAQUS's S4R, S4R5 and S9R5 curved shell element models. All of them are *R*educed-integrated elements with hourglass control and their features are summarized in Table 1. In particular, the formulation of S4R changes when the shell thickness increases from that of the discrete Kirchhoff shell to that of the thick shell. On the other hand, both S4R5 and S9R5 are only recommended for thin shell analysis [50]. In nearly all problems, the deformed structures will be portrayed and the displacement amplification factor is always taken to be unity.

Table 1. Features of S4R, S4R5 and S9R5 curved shell element models.

	S4R	S4R5	S9R5
No. of nodes per element	4	4	9
No. of d.o.f.s per node	6	5	5
Hourglass treatment	default stabilization	default stabilization	default stabilization
Drilling rotation treatment	default stabilization	not applicable	not applicable
Lagrangian framework	updated	total	total
Applicable strain	finite/large	small	small
Intended thickness	thin and thick	thin only	thin only

When the default automatic load incrementation scheme is adopted, the solution procedures of S4R5 are aborted before the load reaches its maximum in many benchmark problems. The situation of S9R5 is even worse. When equal load increments are imposed, S4R5 and S9R5 require considerably larger number of load increments than that of S4R for securing the ultimate solution. In this light, only the predictions of S4R and the related NINC and NITER output at the end of the automatic load incrementation scheme will be reported.

To ensure that the reported solutions have been sufficiently converged with respect to the mesh density, the mesh is refined until the solutions yielded by two successively refined meshes are practically identical. To illustrate that the mesh density is adequate, results predicted by two different meshes will be shown in all load-deflection curves. The two sets of results are graphically indistinguishable and the discrepancy is typically around 0.1%. The precise relations between the applied loads and the selected deflections in numerical format are mostly reported at a load interval given as 5% of the maximum load. If deemed to be necessary, additional data points are employed to enhance the quality of the so-constructed load-deflection curves. Lastly, all problems are geometric nonlinear in the narrow sense and material nonlinearity is not considered.

3.1 Cantilever subjected to End Shear Force

Figure 2a shows a cantilever subjected to the end shear force P. The problem has been considered in references [5,8,19,21,29,32,35,36,45,47,48], among others. A commonly employed mesh for four-node shell elements is 8×1 which is also adequate for the S4R element. Figure 2b plots the end shear force against the vertical and horizontal tip deflections. Table 2a lists the same deflections whereas Table 2b lists the NINC and NITER. Figure 2c portrays the deformed cantilever under the maximum load.

Table 2a. Horizontal and vertical tip deflections for the cantilever loaded with end shear force (computed by using 16×1 S4R elements and NINC* = 40), see Figure 2a.

P/P_{max}	$-U_{tip}$	W_{tip}	P/P_o	$-U_{tip}$	W_{tip}	P/P_o	$-U_{tip}$	W_{tip}
0.05	0.026	0.663	0.40	1.184	4.292	0.75	2.541	6.031
0.10	0.103	1.309	0.45	1.396	4.631	0.80	2.705	6.190
0.15	0.224	1.922	0.50	1.604	4.933	0.85	2.861	6.335
0.20	0.381	2.493	0.55	1.807	5.202	0.90	3.010	6.467
0.25	0.563	3.015	0.60	2.002	5.444	0.95	3.151	6.588
0.30	0.763	3.488	0.65	2.190	5.660	1.00	3.286	6.698
0.35	0.971	3.912	0.70	2.370	5.855			

Table 2b. NINCs and NITERs required to obtained the ultimate solution for the cantilever loaded with end shear force, see Figure 2a.

	8×1 S4R elements	16×1 S4R elements
NINC	15	15
NITER	78	80

3.2 Cantilever subjected to End Moment

Figure 3a shows a cantilever subjected to end moment M. A commonly employed mesh for four-node shell elements is 12×1. The problem has been considered in references [5,10,13,17,18,21,29, 30,32,34,36,40,46], among others. The cantilever forms a circular arc with its radius R given by the classical flexural formula $R = EI/M$. Using the formula, the analytical normalized deflections can be derived to be

$$\frac{U}{L} = \frac{M_o}{M}\sin\frac{M}{M_o} - 1 \quad , \quad \frac{W}{L} = \frac{M_o}{M}(1 - \cos\frac{M}{M_o})$$

where $M_o = EI/L$. The maximum end moment M_{max} is taken to be πM_o at which the beam will be bent into a circle. In this problem, accurate predictions can be yielded by 8×1 S4R elements. Figure 3b plots the end moment against the vertical and horizontal tip deflections. Figure 3c portrays the

deformed cantilevers at M = $0.35M_{max}$, $0.7M_{max}$ and M_{max}. Table 3a lists the analytical and computed tip deflections, which are highly consistent with each other. Table 3b lists the NINC and NITER. Compared to the last cantilever problem, the present one converges less readily.

Table 3a. Horizontal and vertical tip deflections for the cantilever loaded with end bending moment (computed by using 16×1 S4R elements and NINC* = 80), see Figure 3a.

M/M_{max}	$-U_{tip}$		W_{tip}		M/M_{max}	$-U_{tip}$		W_{tip}	
	S4R	exact	S4R	exact		S4R	exact	S4R	exact
0.05	0.196	0.196	1.870	1.870	0.55	13.075	13.073	6.788	6.775
0.10	0.773	0.774	3.648	3.648	0.60	13.875	13.871	5.772	5.758
0.15	1.698	1.699	5.249	5.248	0.65	14.384	14.377	4.678	4.665
0.20	2.916	2.918	6.600	6.598	0.70	14.603	14.595	3.583	3.571
0.25	4.357	4.361	7.643	7.639	0.75	14.556	14.546	2.556	2.546
0.30	5.942	5.945	8.338	8.333	0.80	14.280	14.270	1.656	1.650
0.35	7.582	7.585	8.671	8.664	0.85	13.826	13.818	0.931	0.926
0.40	9.191	9.194	8.646	8.637	0.90	13.254	13.247	0.407	0.405
0.45	10.687	10.688	8.291	8.281	0.95	12.625	12.621	0.099	0.098
0.50	12.000	12.000	7.652	7.639	1.00	12.000	12.000	0.000	0.000

Table 3b. NINCs and NITERs required to obtain the ultimate solution for the cantilever loaded with end bending moment, see Figure 3a.

	8×1 S4R elements	16×1 S4R elements
NINC	125	125
NITER	715	714

3.3 Slit Annular Plate subjected to Lifting Line Force

The slit annular plate is shown in Figure 4a. The problem has been considered in references [23,25,27,33,36,39,40,44,46,48,49], among others. The line force P is applied at one end of the slit while the other end of the slit is fully clamped. A commonly employed mesh for four-node shell elements is 6×30 which is also adequate for the S4R element. Figure 4b plots the load against the vertical deflections at the tips of the slit A and B. Table 4a lists the deflections whereas Table 4b lists the NINC and NITER. Figure 4c shows the deformed slit plate under the maximum load.

Table 4a. Vertical deflections at points A and B of the slit annular plate lifted by a line force (10×80 S4R elements and NINC* = 640), see Figure 4a.

P/P_{max}	W_A	W_B	P/P_{max}	W_A	W_B	P/P_{max}	W_A	W_B
0.025	1.305	1.789	0.30	8.340	11.213	0.70	11.970	15.469
0.05	2.455	3.370	0.35	8.974	11.992	0.75	12.310	15.842
0.075	3.435	4.720	0.40	9.529	12.661	0.80	12.642	16.202
0.10	4.277	5.876	0.45	10.023	13.247	0.85	12.966	16.550
0.125	5.007	6.872	0.50	10.468	13.768	0.90	13.282	16.886
0.15	5.649	7.736	0.55	10.876	14.240	0.95	13.590	17.212
0.20	6.725	9.160	0.60	11.257	14.674	1.00	13.891	17.528
0.25	7.602	10.288	0.65	11.620	15.081			

Table 4b. NINCs and NITERs required to obtain the ultimate solution for slit annular plate lifted by line force, see Figure 4a.

	6×30 S4R elements	10×80 S4R elements
NINC	61	67
NITER	327	346

3.4 Hemispherical Shell subjected to Alternating Radial Forces

Figure 5a shows hemispherical shell with an 18^o circular cutout at its pole. The shell is loaded by alternating radial point forces Ps at 90^o intervals. The problem has been considered in references [18,19,21,23,25,26,28,31,32,34,35,37,40,41,44-49], among others. Owing to symmetry, one quarter of the shell is modeled and a commonly employed mesh for four-node shell elements is 16×16. Figure 5b plots the load against the radial deflections at the points of loading A and B. Table 5a lists the same deflections whereas Table 5b lists the NINC and NITER. Figure 5a also shows the deformed hemispherical shell under the maximum load. In this problem, reasonably accurate predictions can be yielded by using 12×12 S4R elements.

Table 5a. Radial deflections at points A and B of the hemispherical shell problem (computed by 16×16 S4R elements and NINC* = 40), see Figure 5a.

P/P_{max}	V_A	$-U_B$	P/P_{max}	V_A	$-U_B$	P/P_{max}	V_A	$-U_B$
0.05	0.855	0.955	0.40	3.158	5.196	0.75	3.816	7.234
0.10	1.499	1.840	0.45	3.291	5.565	0.80	3.875	7.448
0.15	1.969	2.604	0.50	3.406	5.902	0.85	3.929	7.647
0.20	2.321	3.261	0.55	3.508	6.212	0.90	3.979	7.835
0.25	2.596	3.833	0.60	3.598	6.497	0.95	4.025	8.011
0.30	2.819	4.339	0.65	3.678	6.761	1.00	4.067	8.178
0.35	3.002	4.790	0.70	3.750	7.006			

Table 5b. NINCs and NITERs required to obtain the ultimate solution for the hemisphere shell problem, see Figure 5a.

	12×12 S4R elements	16×16 S4R elements
NINC	27	27
NITER	140	136

3.5 Pullout of an Open-Ended Cylindrical Shell

Figure 6a shows an open-ended cylinder being pulled by a pair of radial forces Ps. The problem has been considered in references [14,24,26,28,32,33,40,44,46,48,49], among others. Owing to symmetry, one-eighth of the shell is modeled and a commonly employed mesh for four-node shell elements is 8×12. Figure 6b plots the load against the radial deflections at points A, B and C. Table 6a lists the data points whereas Table 6b lists the NINC and NITER. The deformed geometry under the maximum load is portrayed in Figure 6c. In this problem, reasonably accurate predictions can

be yielded by 16×24 S4R elements.

Table 6a. Radial deflections at points A, B and C of the open-ended cylindrical shell (computed by using 24×36 S4R elements and NINC* = 400), see Figure 6a.

P/P_{max}	W_A	$-U_B$	$-U_C$	P/P_{max}	W_A	$-U_B$	$-U_C$	P/P_{max}	W_A	$-U_B$	$-U_C$
0.025	0.819	0.864	0.872	0.35	2.321	3.342	3.556	0.70	2.672	4.385	3.378
0.05	1.260	1.471	1.493	0.40	2.376	3.443	3.632	0.75	2.692	4.423	3.353
0.075	1.527	1.901	1.946	0.45	2.425	3.539	3.688	0.80	2.710	4.455	3.332
0.10	1.707	2.217	2.293	0.50	2.473	3.653	3.718	0.85	2.726	4.483	3.313
0.15	1.936	2.641	2.792	0.525	2.543	4.061	3.580	0.90	2.741	4.508	3.297
0.20	2.079	2.904	3.106	0.55	2.577	4.171	3.518	0.95	2.755	4.530	3.283
0.25	2.180	3.087	3.310	0.60	2.618	4.274	3.452	1.00	2.768	4.551	3.269
0.30	2.257	3.227	3.452	0.65	2.648	4.338	3.410				

Table 6b. NINCs and NITERs required to obtain the ultimate solution for the open-ended cylindrical shell, see Figure 6a.

	16×24 S4R elements	24×36 S4R elements
NINC	18	18
NITER	91	94

3.6 Pinched Cylindrical Shell mounted over Rigid Diaphragms

Figure 7a shows a pinched cylindrical shell mounted on rigid end diaphragms over which the in-plane displacements U and W are restrained. The problem and its variations have been considered in references [21,26,37,43-45,48], among others. Owing to symmetry, one-eighth of the shell is modeled and a commonly employed mesh for four-node shell elements is 40×40 which is also adequate for the S4R element. Figure 7b plots the load against radial deflections at points A and B. Table 7a lists the same deflections whereas Table 7b lists the NINC and NITER. The deformed geometry under the maximum load is portrayed in Figure 7c.

Table 7a. Radial deflections at points A and B of the pinched cylindrical shell (computed by 48×48 S4R elements and NINC* =1280), see Figure 7a.

P/P_{max}	$-W_A$	U_B	P/P_{max}	$-W_A$	U_B	P/P_{max}	$-W_A$	U_B
0.05	9.561	-0.233	0.30	65.498	17.979	0.70	78.451	29.772
0.075	15.648	-0.922	0.35	68.229	20.365	0.75	79.339	30.604
0.10	23.164	-2.391	0.40	70.424	22.321	0.80	80.218	31.471
0.125	29.375	-3.872	0.45	72.204	23.916	0.85	81.045	32.299
0.15	36.208	-2.154	0.50	73.790	25.381	0.90	81.766	32.989
0.175	51.499	6.792	0.55	75.139	26.631	0.95	82.435	33.619
0.20	56.373	10.448	0.60	76.331	27.735	1.00	83.102	34.272
0.25	61.877	14.905	0.65	77.472	28.843			

Table 7b. NINCs and NITERs required to obtain the ultimate solution for the pinched cylindrical shell, see Figure 7a.

	40×40 S4R elements	48×48 S4R elements
NINC	69	70
NITER	391	406

3.7 Pinched Semi-Cylindrical Isotropic and Laminated Shells

Figure 8a shows the semi-cylindrical shell subjected to an end pinching force at the middle of the free-hanging circumferential periphery. The other circumferential periphery is fully clamped. Along its longitudinal edges, the vertical deflection and the rotation about the Y-axes are restrained. Besides the isotropic material, laminates with stacking sequences $[0^0/90^0/0^0]$ and $[90^0/0^0/90^0]$ are also considered. In the laminates, all plies are equal in thickness. A ply is of 0^0 if its fibres are parallel to the longitudinal direction of the shell. The present problems have been considered in references [16,22,33,40,42,47,48], among others. Owing to symmetry, half of shell is modeled and a commonly employed mesh for four-node shell elements is 16×16. Figure 8b plots the applied force against the downward deflections at A. Table 8a lists the same deflections whereas Table 8b lists the NINC and NITER. The deformed shells under the maximum load are portrayed in Figures 8c and 8d. In this problem, reasonably accurate predictions can be yielded by 32×32 S4R elements.

Table 8a. The downward deflection at A of the pinched semi-cylindrical shells (computed by using 40×40 S4R elements and NINC* = 320), see Figure 8a.

P/P_{max}	isotropic	$[0^0/90^0/0^0]$	$[90^0/0^0/90^0]$	P/P_{max}	isotropic	$[0^0/90^0/0^0]$	$[90^0/0^0/90^0]$
0.05	5.421	15.340	7.558	0.45	124.751	177.404	132.488
0.10	16.100	37.920	22.722	0.50	132.653	180.680	138.740
0.125	22.195	55.145	30.594	0.55	138.920	183.544	144.238
0.15	27.657	93.433	37.897	0.60	144.185	186.099	149.191
0.175	32.700	129.575	45.427	0.65	148.770	188.415	153.728
0.20	37.582	141.562	54.455	0.70	152.863	190.543	157.930
0.225	42.633	149.034	65.814	0.75	156.584	192.520	161.854
0.25	48.537	154.634	79.512	0.80	160.015	194.376	165.540
0.275	56.355	159.141	92.524	0.85	163.211	196.132	169.017
0.30	66.410	162.896	102.357	0.90	166.200	197.808	172.308
0.325	79.810	166.099	109.793	0.95	168.973	199.420	175.430
0.35	94.669	168.884	115.746	1.00	171.505	200.983	178.386
0.40	113.704	173.560	125.094				

Table 8b. NINCs and NITERs required to obtain the ultimate solution for the pinched semi-cylindrical, see Figure 8a.

	32×32 S4R elements			40×40 S4R elements		
	isotropic	$[0^0/90^0/0^0]$	$[90^0/0^0/90^0]$	isotropic	$[0^0/90^0/0^0]$	$[90^0/0^0/90^0]$
NINC	28	36	32	28	36	33
NITER	136	171	184	136	170	184

3.8 Hinged Cylindrical Isotropic and Laminated Roofs

Figure 9a shows the hinged semi-cylindrical roof subjected to a central pinching force. An isotropic material, $[0^0/90^0/0^0]$ laminate and $[90^0/0^0/90^0]$ laminate at two different thicknesses are considered. Again, a ply is of 0^0 if its fibres are parallel to the longitudinal direction of the shell. All plies in the same laminate are equal in thickness. Along the hinged edges, all nodal translations are restrained. These problems have been considered in references [4-12,15,17,18,20,21,24,26,28-30,33,36,38,43,47,48], among others, and are particularly popular due to the snapping behavior. At some intermediate state, the tangential global stiffness matrices become singular. The problems are often, if not always, solved by Riks solution method and such an option in ABAQUS is adopted. Owing to symmetry, one quarter of the roof is modeled and a commonly employed mesh for four-node shell elements is 4×4. For the 12.7 unit thick shells, reasonably accurate predictions can be yielded by using 8×8 S4R elements as shown in Figure 9b. For the 6.35 unit thick shells, the same mesh is inadequate. However, reasonably accurate predictions can be obtained by using 16×16 S4R elements as shown in Figure 9c. Tables 9a to 9f list the data points. With the Riks solution method, it is not possible to yield a solution at a preset load level. This explains why the load levels in the tables are different whereas the load-deflections curves produced by the coarser meshes do not reach the last solution points yielded by the finer meshes in Figures 9b and 9c. Despite the high nonlinearity, the maximum deflections are much smaller than the overall dimensions of the roof. Unlike the previous problems, the deformed meshes are not shown as they can hardly be distinguished from the undeformed ones. As the default automatic load incrementation scheme does not work for the present problems, there are no NINC and NITER.

Table 9a. Deflections for the 12.7 unit thick isotropic hinged cylindrical shell (computed by using 16×16 S4R elements and Riks method), see Figure 9a.

P/P_{max}	$-W_C$	P/P_{max}	$-W_C$	P/P_{max}	$-W_C$	P/P_{max}	$-W_C$
0.0877	0.693	0.7421	11.293	0.3245	16.590	0.3871	24.049
0.1980	1.638	0.7286	12.141	0.2717	17.094	0.4443	24.663
0.3473	3.087	0.7023	12.903	0.2272	17.657	0.5093	25.293
0.4686	4.477	0.6649	13.583	0.1940	18.299	0.5826	25.940
0.5647	5.802	0.6182	14.188	0.1750	19.028	0.6644	26.601
0.6381	7.057	0.5643	14.728	0.1729	19.852	0.7551	27.276
0.6908	8.237	0.5055	15.217	0.1905	20.771	0.8549	27.964
0.7246	9.339	0.4442	15.676	0.2303	21.780	0.9643	28.663
0.7412	10.358	0.3830	16.125	0.2950	22.875	1.0835	29.374

Table 9b. Deflections for the 12.7 unit thick [$0^0/90^0/0^0$] hinged cylindrical shell (computed by using 16×16 S4R elements and Riks method), see Figure 9a.

P/P_{max}	$-W_C$	P/P_{max}	$-W_C$	P/P_{max}	$-W_C$	P/P_{max}	$-W_C$
0.0546	0.807	0.3577	10.735	0.0638	16.199	0.0194	22.707
0.1245	1.956	0.3464	11.516	0.0303	16.648	0.0697	23.824
0.1938	3.281	0.3288	12.227	0.0007	17.141	0.1354	25.005
0.2494	4.548	0.3057	12.872	-0.0236	17.692	0.2178	26.244
0.2925	5.753	0.2778	13.458	-0.0411	18.317	0.3181	27.533
0.3244	6.892	0.2461	13.990	-0.0504	19.024	0.4374	28.864
0.3459	7.961	0.2115	14.477	-0.0503	19.817	0.5769	30.229
0.3582	8.959	0.1749	14.928	-0.0394	20.698	0.7374	31.622
0.3618	9.884	0.0999	15.774	-0.0165	21.663	1.0192	33.748

Table 9c. Deflections for the 12.7 unit thick [$90^0/0^0/90^0$] hinged cylindrical shell (computed by using 16×16 S4R elements and Riks method), see Figure 9a.

P/P_{max}	$-W_C$	P/P_{max}	$-W_C$	P/P_{max}	$-W_C$	P/P_{max}	$-W_C$
0.0556	0.649	0.5336	9.545	0.5801	16.019	0.2834	20.881
0.1299	1.581	0.5550	10.404	0.5685	16.545	0.2789	21.318
0.2090	2.673	0.5716	11.231	0.5542	17.028	0.2812	21.823
0.2784	3.740	0.5838	12.024	0.5374	17.465	0.3099	23.030
0.3389	4.781	0.5919	12.782	0.4971	18.206	0.3755	24.476
0.3914	5.794	0.5963	13.505	0.4498	18.785	0.4832	26.120
0.4365	6.777	0.5970	14.192	0.3991	19.249	0.6380	27.921
0.4748	7.731	0.5945	14.841	0.3501	19.682	0.8444	29.844
0.5070	8.654	0.5888	15.450	0.3090	20.191	1.0356	31.349

Table 9d. Deflections for the 6.35 unit thick isotropic hinged cylindrical shell (computed by using 24×24 S4R elements and Riks method), see Figure 9a.

P/P_{max}	$-W_C$	P/P_{max}	$-W_C$	P/P_{max}	$-W_C$	P/P_{max}	$-W_C$
0.0517	1.846	0.1671	15.501	-0.1001	14.520	-0.0006	24.824
0.1182	5.271	0.1323	16.145	-0.1142	14.451	0.0626	26.565
0.1583	8.257	0.0923	16.602	-0.1247	14.862	0.1427	28.302
0.1837	10.799	0.0504	16.915	-0.1288	15.778	0.2403	30.023
0.1914	11.904	0.0083	17.008	-0.1271	16.961	0.3559	31.720
0.1953	12.892	-0.0312	16.697	-0.1196	18.320	0.4898	33.388
0.1950	13.752	-0.0622	15.780	-0.1055	19.817	0.6417	35.024
0.1901	14.472	-0.0739	15.206	-0.0825	21.420	0.8114	36.626
0.1806	15.050	-0.0861	14.767	-0.0484	23.100	1.0313	38.450

Table 9e. Deflections for the 6.35 unit thick [$0^0/90^0/0^0$] hinged cylindrical shell (computed by using 24×24 S4R elements and Riks method), see Figure 9a.

P/P_{max}	$-W_C$	P/P_{max}	$-W_C$	P/P_{max}	$-W_C$	P/P_{max}	$-W_C$
0.0423	3.414	-0.0817	15.574	0.0593	11.860	-0.0731	17.712
0.0765	8.834	-0.0779	12.857	0.0428	10.506	-0.0593	20.694
0.0782	12.280	-0.0650	10.991	0.0210	10.406	-0.0214	24.230
0.0564	14.492	-0.0442	10.126	-0.0006	10.745	0.0556	27.809
0.0271	16.397	-0.0189	10.494	-0.0215	11.263	0.1700	31.174
-0.0059	18.017	0.0007	11.931	-0.0419	11.861	0.3213	34.362
-0.0240	18.602	0.0142	13.623	-0.0607	12.555	0.5085	37.394
-0.0436	18.875	0.0296	14.751	-0.0742	13.602	0.7292	40.274
-0.0657	18.365	0.0499	14.425	-0.0780	15.332	1.0243	43.444

Table 9f. Deflections for the 6.35 unit thick [$90^0/0^0/90^0$] hinged cylindrical shell (computed by using 24×24 S4R elements and Riks method), see Figure 9a.

P/P_{max}	$-W_C$	P/P_{max}	$-W_C$	P/P_{max}	$-W_C$	P/P_{max}	$-W_C$
0.0490	2.699	0.1499	18.140	-0.0117	14.369	-0.0402	22.448
0.0822	5.205	0.1385	18.954	-0.0168	13.519	0.0036	24.905
0.1063	7.479	0.1222	19.416	-0.0297	13.456	0.0693	27.427
0.1249	9.527	0.1019	19.429	-0.0458	13.873	0.1598	29.941
0.1393	11.374	0.0792	19.167	-0.0619	14.469	0.2761	32.401
0.1498	13.043	0.0331	18.249	-0.0752	15.258	0.4180	34.786
0.1562	14.550	0.0134	17.555	-0.0818	16.461	0.5847	37.088
0.1585	15.905	-0.0011	16.641	-0.0792	18.129	0.7747	39.301
0.1565	17.107	-0.0088	15.532	-0.0663	20.157	1.0234	41.773

4. CLOSURE

From more than forty publications on geometric nonlinear analysis of shells, eight sets of popularly employed benchmark problems are identified and the detailed reference solutions are tabulated. It is hoped that the solutions will form a convenient basis for subsequent comparison and that the inaccurate and time consuming task of reconstructing data points by graphical measurement of previously reported load-deflection curves can be avoided. To reveal the relative convergent difficulty, the number of load increments (NINC) and the number iterations (NITER) required by an automatic load incrementation scheme to attain the maximum loads are also reported. Care has been exercised to ensure that the reported solutions have been highly converged with respect to the mesh density. It is interesting to note that once the employed mesh becomes sufficiently fine, the NINC and the NITER are not sensitive to further mesh refinement. In view of converging difficulty, the most demanding problems are the cantilever subjected to end moment and the hinged cylindrical roofs. While the hinged roof problems must be solved by Riks method, NINC and NITER of the cantilever problem are significantly higher than that of the remaining benchmark cases.

Acknowledgment – The financial support of the William Mong Engineering Research Fund in form of a young researcher award to the second author is gratefully acknowledged. Mr.W.K.Chan is thanked for preparing some of the preliminary ABAQUS input date files.

REFERENCES

1. MacNeal RH, Harder RL. A proposed standard set of problems to test finite element accuracy. *Finite Elements in Analysis & Design*, **1**, 3–20 (1985)
2. Hitchings D, Kamoulakos A, Davies GAO. Linear statics benchmarks. National Agency for Finite Element Methods & Standards, Glasgow, UK, 1987.
3. Prinja NK, Clegg RA. Assembly benchmark tests for 3-D beams and shells exhibiting geometric non-linear behaviour, NAFEMS, Glasgow, UK, 1993.
4. Sabir AB, Lock AC, The application of finite elements to the large deflection geometrically nonlinear behaviour of cylindrical shells. *Variational Methods in Engineering*, ed. by Brebbia CA, Tottenham H, Southampton University Press, 7/54-7/65, 1972.
5. Horrigmoe G, Bergan PG. Nonlinear analysis of free-from shells by flat finite elements. *Computer Methods Appl.Mech.Engrg.*, **16**: 11-35 (1978)
6. Hughes TJR, Liu WK. Nonlinear finite element analysis of shells: Part I. Three-dimensional shells. *Computer Methods Appl.Mech.Engrg.*, **26**: 331-362 (1981)
7. Crisfield MA. A fast incremental/iterative solution procedure that handles "snap-through". *Computers & Structures*, **13**: 55–62 (1981)
8. Parisch H. Large displacements of shells including material nonlinearities. *Computer Methods Appl.Mech.Engrg.*, **27**: 183-214 (1981)
9. Surana KS. Geometrically non-linear formulation for the three dimensional solid-shell transition finite elements. *Computers & Structures*, **15**: 549-566 (1982)
10. Surana KS. Geometrically nonlinear formulation for curved shell elements. *Inter. J. Numer. Methods Engrg.*, **19**: 581-615 (1983)
11. Oliver J, Onate E. A total Lagrangian formulation for the geometrically nonlinear analysis of structures using finite elements. Part I. Two-dimensional problems: shell and plate structures. *Inter.J. Numer.Methods Engrg.*, **20**: 2253-2281 (1984)
12. Saigal S, Kapania R, Yang Y. Geometric nonlinear finite element analysis of imperfect laminated shells. *J. Composite Mater.*, **20**: 197-214 (1986)
13. Simo JC, Vu-Quoc L. A three-dimensional finite strain rod model, Part II: computational aspects. *Computer Methods Appl.Mech.Engrg.*, **58**: 79-116 (1986)
14. Gruttmann F, Stein E, Wriggers P. Theory and numerics of thin elastic shells with finite rotations. Ingenieur-Archiv, **59**: 54-67 (1989)
15. Yeom CH, Lee SW. An assumed strain finite element model for large deflection composite shells. *Inter.J.Numer.Methods Engrg.*, **28**: 1749-1768 (1989)
16. Stander N, Matzenmiller A and Ramm E. An assessment of assumed strain method in finite rotation shell analysis. *Engrg.Comput.*, **6**: 58-66 (1989)
17. Hsiao KM, Chen YR. Nonlinear analysis of shell structures by degenerated isoparametric shell element. *Computers & Structures*, **31**: 427-438 (1989)
18. Simo JC, Fox DD and Rifai MS. On a stress resultant geometrically exact shell model. Part III: Compuational aspects of the nonlinear theory. *Computer Methods Appl.Mech.Engrg.*, **79**: 21-70 (1990)
19. Simo JC, Rifai MS and Fox DD. On a stress resultant geometrically exact shell model. Part IV: Variable thickness shells with through-the-thickness stretching. *Computer Methods Appl.Mech. Engrg.*, **81**: 91-126 (1990)
20. Laschet G, Jeusette, JP. Postbuckling finite element analysis of composite panels. *Compos. Structure*, **14**: 35-48 (1990)
21. Saleeb AF, Chang TY, Graf W, Yingyeunyong S. A hybrid/mixed model for non-linear shell analysis and its applications to large-rotation problems. *Inter.J.Numer.Methods Engrg.*, **29**: 407–446 (1990)
22. Parisch H. An investigation of a finite rotation four node assumed strain shell element. *Inter.J. Numer.Methods Engrg.*, **31**: 127-150 (1991)

23. Buechter N, Ramm E. Shell theory versus degeneration-a comparison in large rotation finite element analysis. *Inter.J.Numer.Methods Engrg.*, **34**: 39-59 (1992)
24. Peng X, Crisfield MA. A consistent corotational formulation for shells using the constant stress/ constant moment triangle. *Inter.J.Numer.Methods Engrg.*, **35**: 1829-1847 (1992)
25. Basar Y, Ding Y. Finite-rotation shell elements for the analysis of finite-rotation shell problems. *Inter.J.Numer.Methods Engrg.*, **34**: 165–169 (1992)
26. Sansour C, Bufler H. An exact finite rotation shell theory, its mixed variational formulation and its finite element implementation. *Inter.J.Numer.Methods Engrg.*, **34**: 73-115 (1992)
27. Wriggers P, Gruttmann F. Thin shells with finite rotations formulated in Biot stress: Theory and finite element formulation. *Inter.J.Numer.Methods Engrg.*, **36**: 2049-2071 (1993)
28. Jiang L, Chernuka MW. A simple four-noded corotational shell element for arbitrarily large rotations. *Computers & structures*, **53**: 1123–1132 (1994)
29. To CWS and Liu ML. Hybrid strain based three node flat triangular shell elements II: numerical investigation of nonlinear problems. *Computers & Structures*, **54**: 1057-1076 (1995)
30. Flores FG, Onate E, Zarate F. New assumed strain triangles for non linear shell analysis. *Computational Mechanics*, **17**: 107-114 (1995)
31. Parisch H. A continuum-based shell theory for non-linear applications. *Inter.J.Numer.Methods Engrg.*, **38**: 1855-1883 (1995)
32. Park HC, Cho C, Lee SW. An efficient assumed strain element model with six dof per node for geometrically nonlinear shells. *Inter.J.Numer.Methods Engrg.*, **38**: 4101–4122 (1995)
33. Brank B, Peric D, Damjanic FB. On implementation of a nonlinear four node shell finite element for thin multilayered elastic shells. *Computational Mechanics,* **16**: 341-359 (1995)
34. Betsch P, Stein E. An assumed strain approach avoiding artificial thickness straining for a non-linear 4-node shell element. *Commun.Numer.Methods Engrg.*, **11**: 899–909 (1995)
35. Betsch P, Gruttmann F, Stein E. A 4-node finite shell element for the implementation of general hyperelastic 3D-elasticity at finite strains. *Computer Methods Appl.Mech.Engrg.*, **130**: 57–79 (1996)
36. Barut A, Madenci E, Tessler A. Nonlinear analysis of laminates through a Mindlin-type shear deformable shallow shell element. *Computer Methods Appl.Mech.Engrg.*, **143**: 155-173 (1997)
37. Hauptmann R, Schweizerhof K. A systematic development of solid-shell element formulations for linear and non-linear analyses employing only displacement degrees of freedom. *Inter.J.Numer.Methods Engrg.*, **42**, 49–69 (1998)
38. Lee SJ, Kanok-Numkulchai. A nine-node assumed strain finite element for large-deformation analysis of laminated shells. *Inter.J.Numer.Methods Engrg.*, **42**: 777-798 (1998)
39. Sansour C, Bocko J. On hybrid stress, hybrid strain and enhanced strain finite element formulations for a geometrically exact shell theory with drilling degrees of freedom. *Inter.J. Numer.Methods Engrg.*, **43**: 175-192 (1998)
40. Mohan P, Kapania RK. Updated Lagrangian formulation of a flat triangular element for thin laminated shells. *AIAA Journal*, **36**: 273-281 (1998)
41. Providas E, Kattis MA. A simple finite element model for the geometrically nonlinear analysis of thin shells. *Computational Mechanics*, **24**: 127-137 (1999)
42. Klinkel S, Gruttmann F, Wagner W. A continuum based three-dimensional shell element for laminated structures. *Computers & Structures*, **71**: 43–62 (1999)
43. Sze KY, Zheng SJ. A hybrid stress nine-node degenerated shell element for geometric nonlinear analysis. *Computational Mechanics*, **23**: 448-456 (1999)
44. Sansour C, Kollmann FG. Families of 4-node and 9-node finite elements for a finite deformation shell theory. An assessment of hybrid stress, hybrid strain and enhanced strain elements. *Computational Mechanics*, **24**: 435–447 (2000)
45. El-Abbasi N, Meguid SA. A new shell element accounting for through-thickness deformation. *Computer Methods Appl.Mech.Engrg.*, **189**: 841–862 (2000)

46. Hong WI, Kim JH, Kim YH, Lee SW. An assumed strain triangular curved solid shell element formulation for analysis for plates and shells undergoing finite rotations. *Inter.J.Numer.Methods Engrg.*, **52**: 747-761 (2001)
47. Sze KY, Zheng S-J. A stabilized hybrid-stress solid element for geometrically nonlinear homogeneous and laminated shell analyses. *Computer Methods Appl.Mech.Engrg*., **191**: 1945-1966 (2002)
48. Sze KY, Chan WK, Pian THH. An eight-node hybrid-stress solid-shell element for geometric nonlinear analysis of elastic shells. *Inter.J.Numer.Methods Engrg*., **55**: 853-878 (2002)
49. Kim CH, Sze KY, Kim YH. Curved quadratic triangular degenerated- and solid-shell elements for geometric nonlinear analysis. *Inter.J.Numer.Methods Engrg*., **57**: 2077-2097 (2003)
50. ABAQUS. *ABAQUS Theory and User's Manuals, Version 5.8*, Hibbitt, Karlsson & Sorensen, Inc., Pawtucket, Rhode Island, USA, 1998.

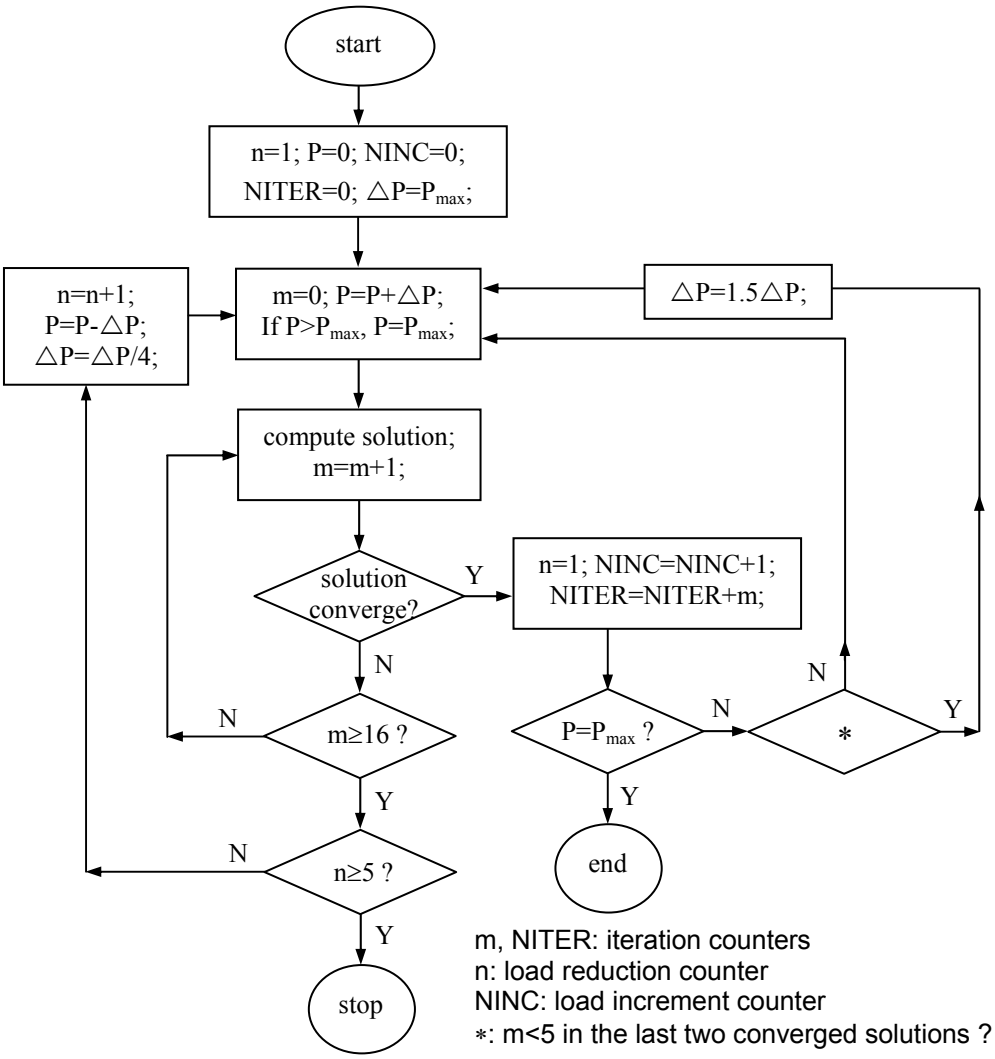

Figure 1. The automatic load incrementation scheme.

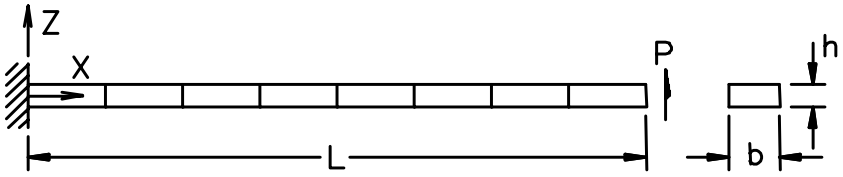

$E=1.2\times10^6$
$\nu = 0,\ L = 10$
$b = 1,\ h = 0.1$
$P_o = EI/L^2 = 1$
$P_{max} = 4P_o = 4$

Figure 2a: Cantilever subjected to end shear force.

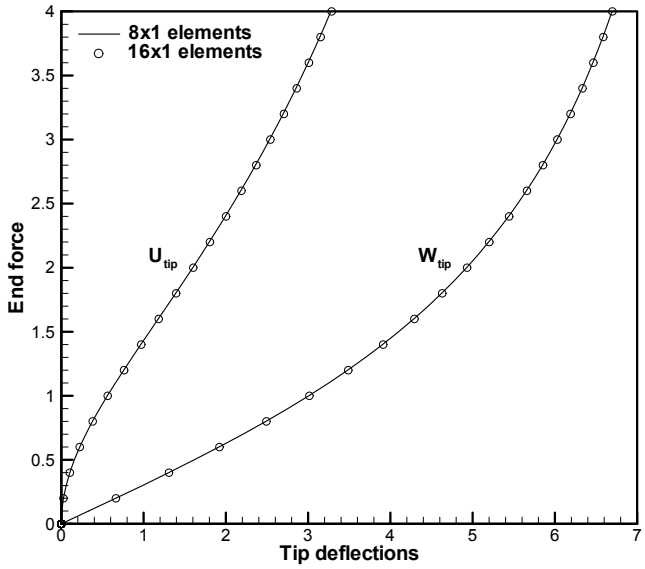

Figure 2b: Load-deflection curves for cantilever subjected to end shear force.

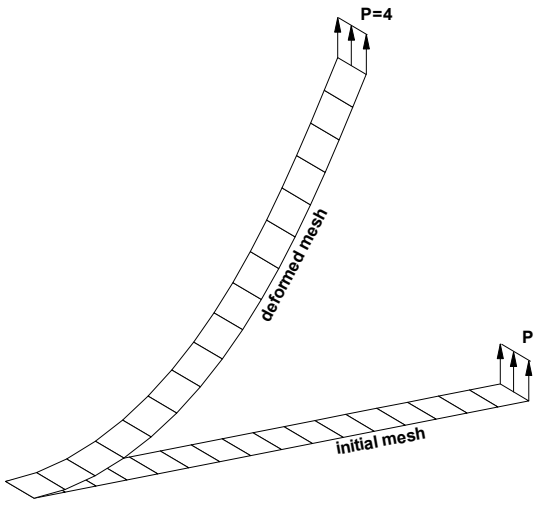

Figure 2c: The deformed 16×1 mesh under the maximum force.

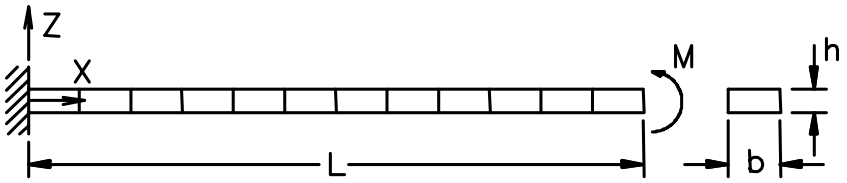

$E=1.2\times10^6$
$\nu = 0,\ L = 12$
$b = 1,\ h = 0.1$
$M_o = EI/L = 25/3$
$M_{max} = 2\pi M_o = 50\pi/3$

Figure 3a. Cantilever subjected to end bending moment.

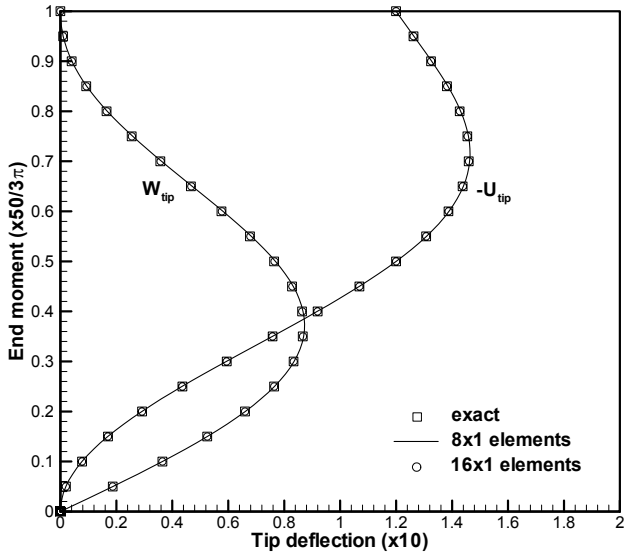

Figure 3b: Load-deflection curves for cantilever subjected to end bending moment.

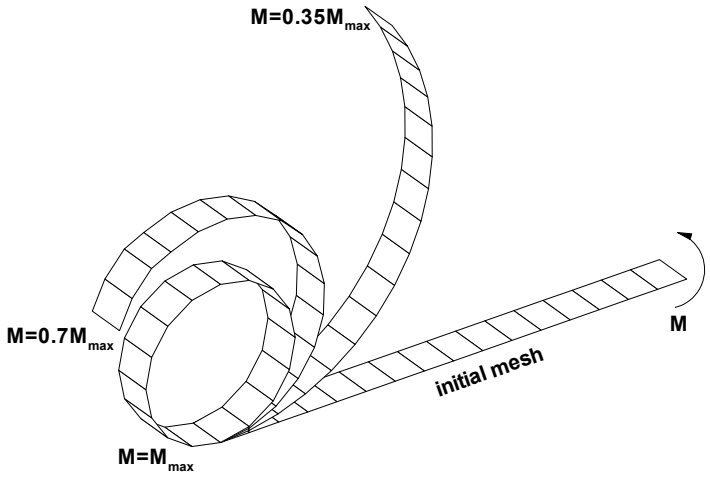

Figure 3c: The deformed 16×1 mesh under the maximum bending moment.

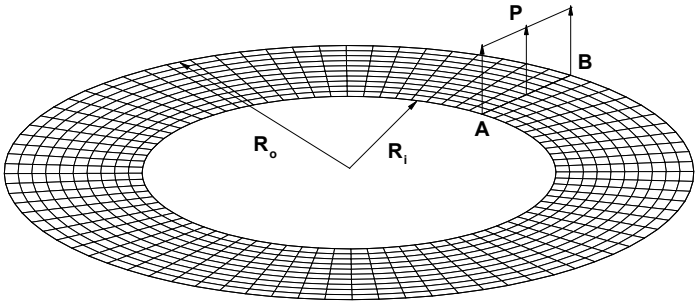

$E = 21\times10^6$,
$\nu = 0$
$R_i = 6$, $R_o = 10$
$h = 0.03$
$P_{max} = 0.8$ (force/length)

Figure 4a. The slit annular plate loaded with the line force P.

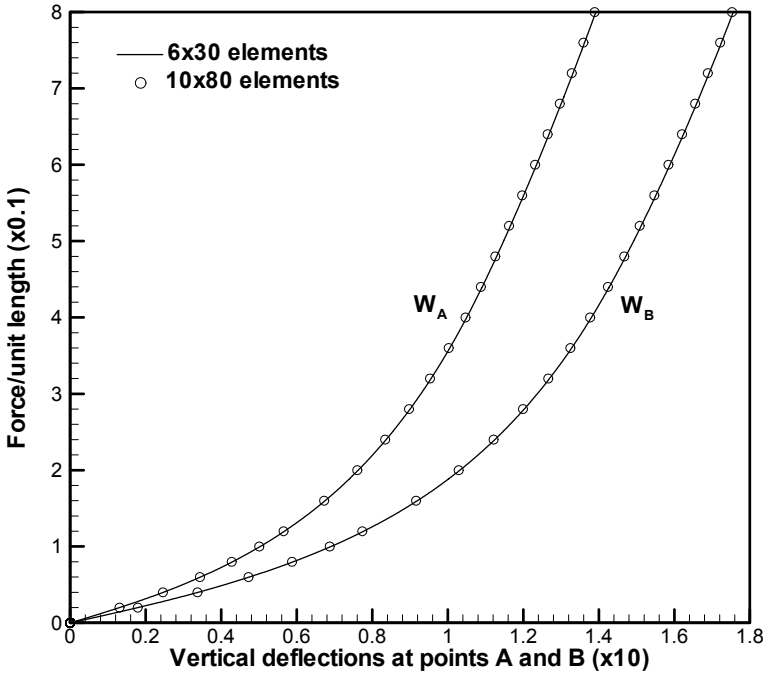

Figure 4b: Load-deflection curves for the slit annular plate lifted by line force P.

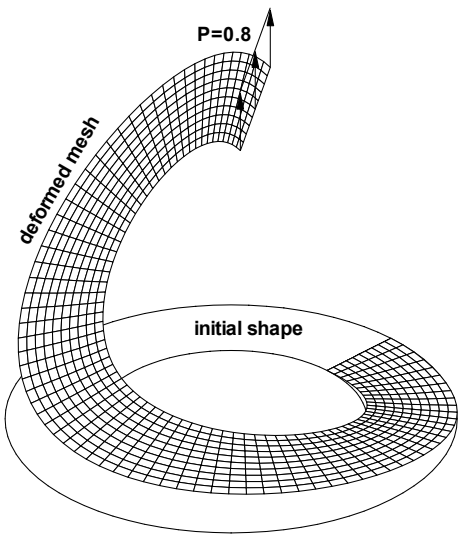

Figure 4c: The deformed 10×80 mesh at $P=P_{max}$.

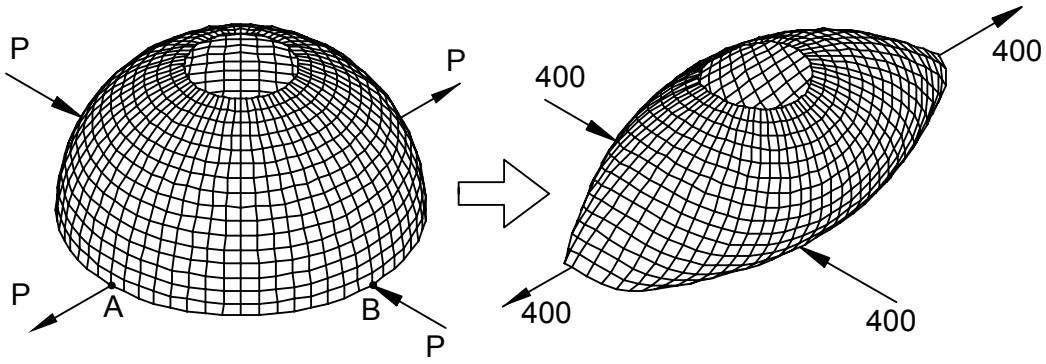

$E = 6.825\times10^7$
$\nu = 0.3$
$R = 10$
$h = 0.04$
$P_{max} = 400$

Figure 5a. The initial geometry and deformed geometry at $P = P_{max}$ for the hemispherical shell subjected to inward and outward radial forces.

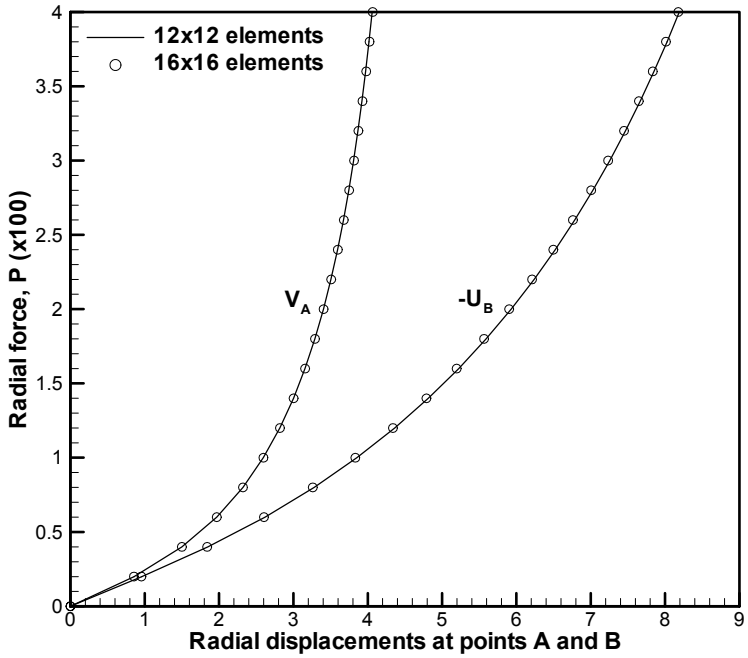

Figure 5b: Load-deflection curves for the hemisphere shell subjected to radial forces.

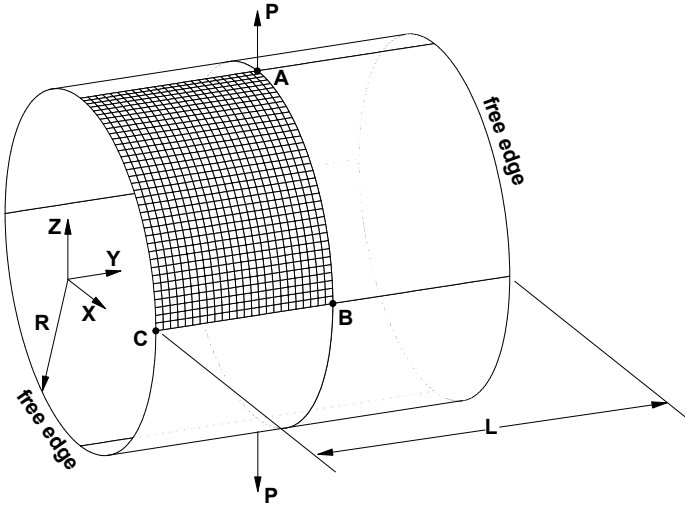

$E = 10.5\times10^6$
$\nu = 0.3125$
$R = 4.953$
$L = 10.35$
$h = 0.094$
$P_{max} = 40{,}000$

Figure 6a: The open-end cylindrical shell subjected to radial pulling forces.

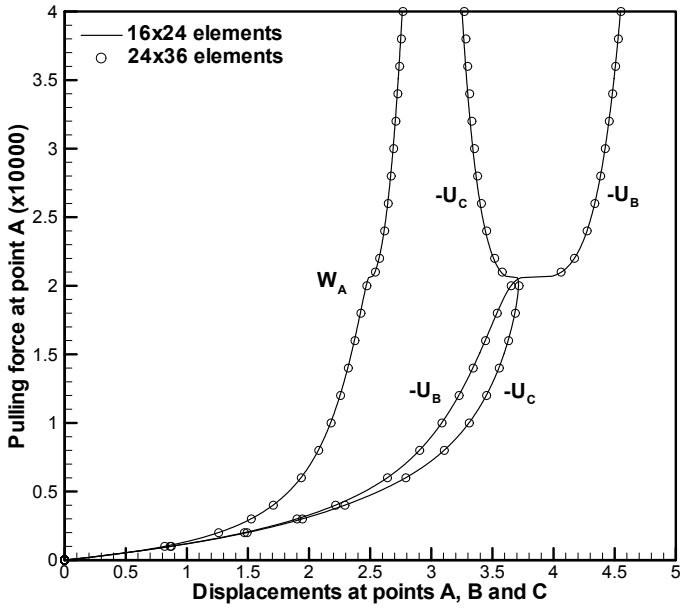

Figure 6b: Load-deflection curves of the open-end cylinder subjected to pulling forces.

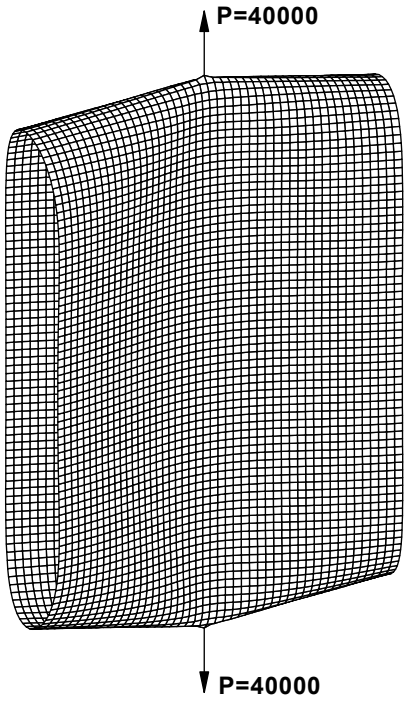

Figure 6c: The deformed 24×36 mesh for the open-ended cylindrical under the maximum load.

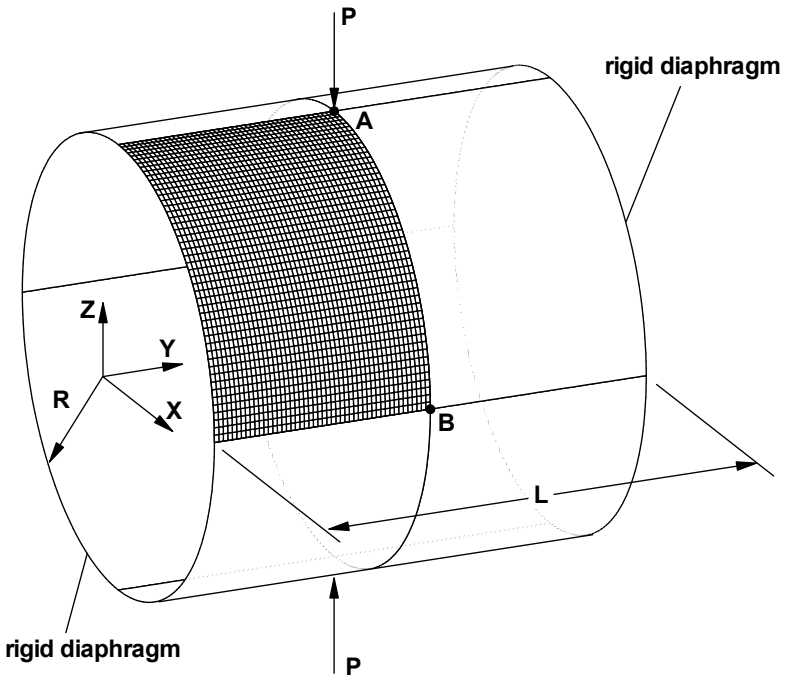

$E = 30\times10^3$
$\nu = 0.3$
$R = 100$
$L = 200$
$h = 1$
$P_{max} = 12{,}000$

Figure 7a: Pinched cylindrical shell mounted on rigid end diaphragms.

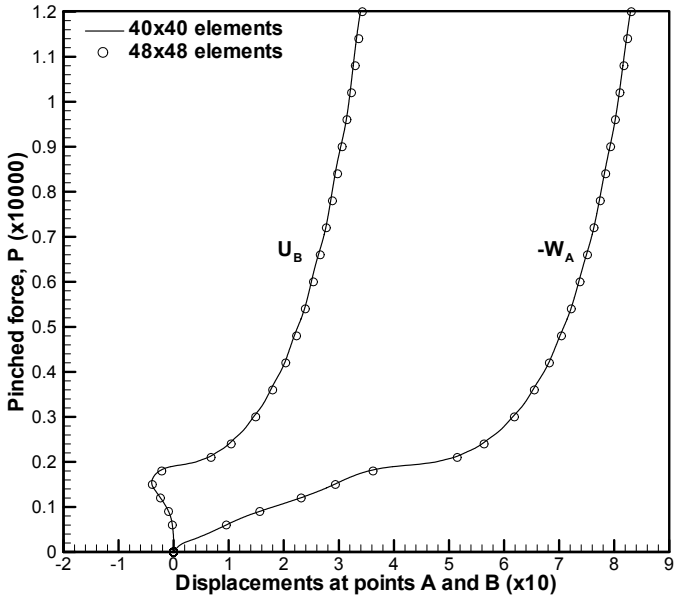

Figure 7b: Load-deflection curves of the pinched cylinder mounted over rigid end diaphragms.

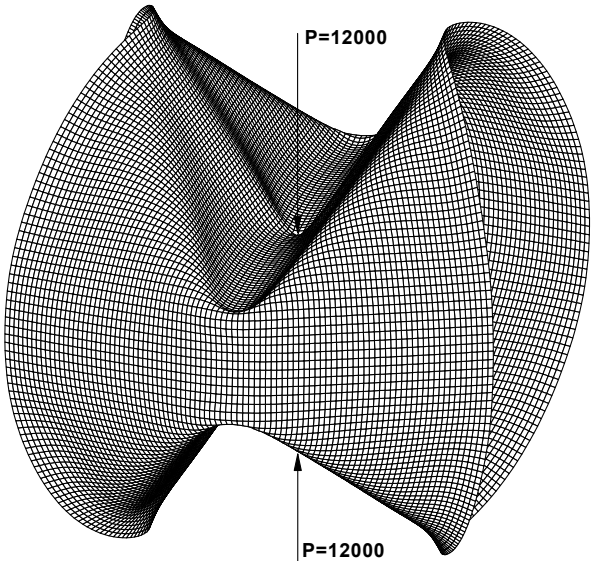

Figure 7c: The deformed 48×48 mesh of the pinched cylinder under maximum load.

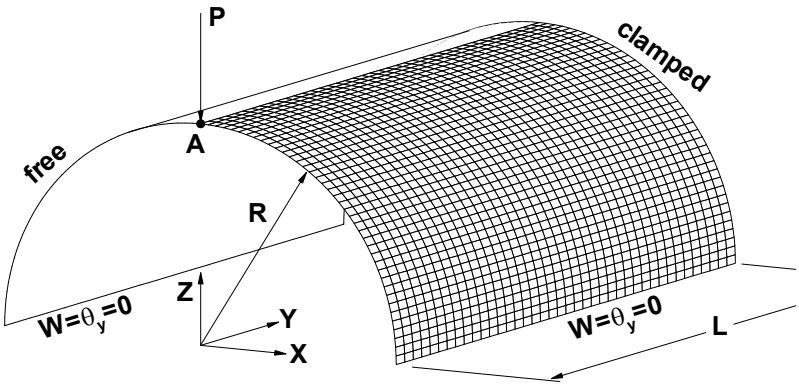

Isotropic Shell

$E=2.0685\times10^7$, $\nu=0.3$

Laminated Shell

$E_L = 2068.5$, $E_T = 517.125$
$G_{LT} = 795.6$, $\nu_{LT} = \nu_{TT} = 0.3$
lamination: $[0^0/90^0/0^0]$ and $[90^0/0^0/90^0]$

Figure 8a. The semi-cylindrical shell subjected to an end pinching force.

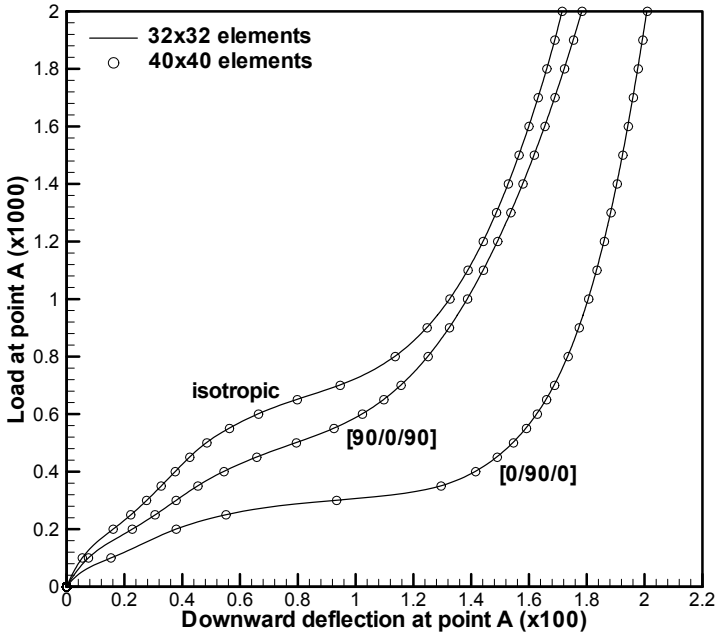

Figure 8b: Load-deflection curves of the semi-cylindrical shell subjected to end pinching force.

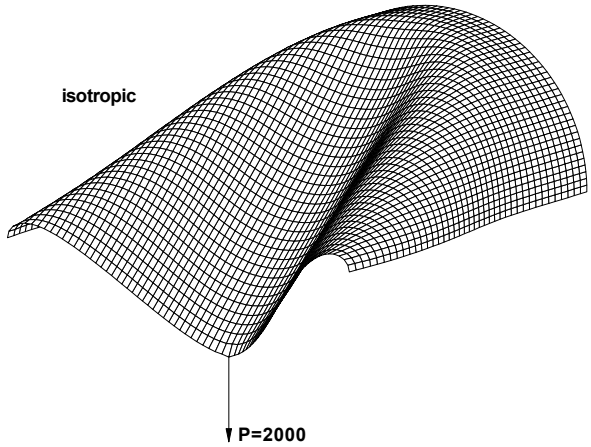

Figure 8c. The deformed 40×40 mesh of the semi-cylindrical isotopic shell under maximum load.

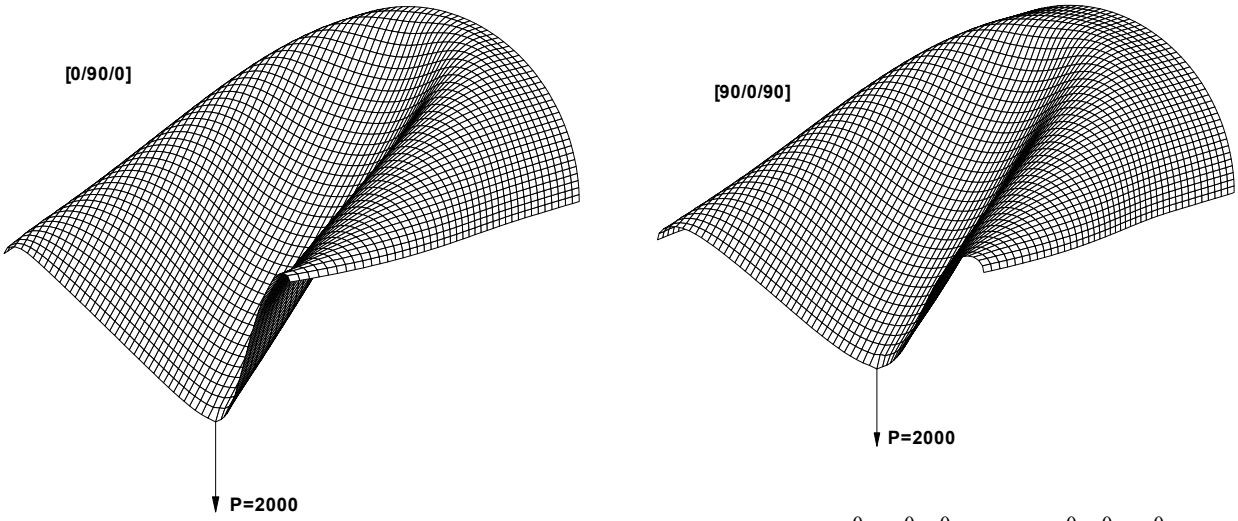

Figure 8d. The deformed 40×40 meshes of the semi-cylindrical $[0^0/90^0/0^0]$ and $[90^0/0^0/90^0]$ laminated shells under maximum load.

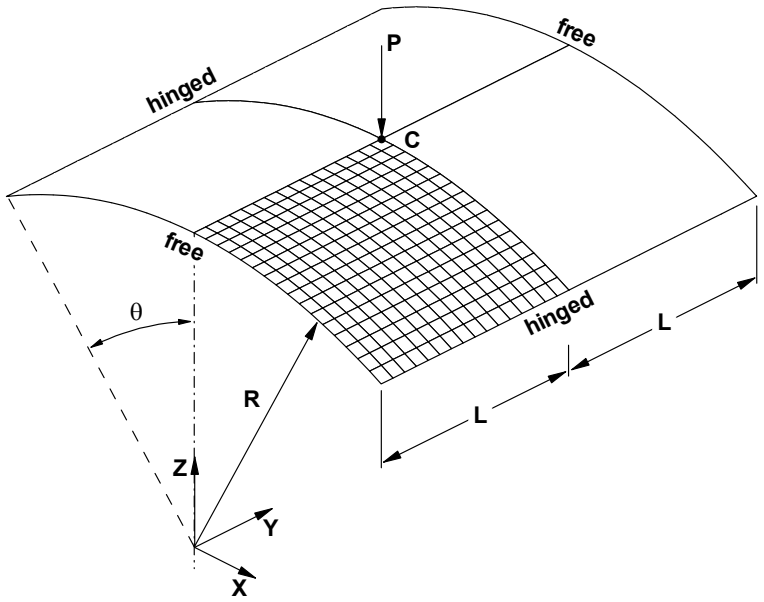

R = 2540, L = 254
θ = 0.1 radian
h = 12.7 or 6.35
P_{max} = 3000

Isotropic Shell
E = 3102.75 , ν = 0.3

Laminated Shell
E_L = 3300, E_T = 1100
G_{LT} = 660, $\nu_{LT} = \nu_{TT}$ = 0.25
lamination: $[0^0/90^0/0^0]$ and $[90^0/0^0/90^0]$

Figure 9a: Hinged cylindrical roof subjected to a central pinching force.

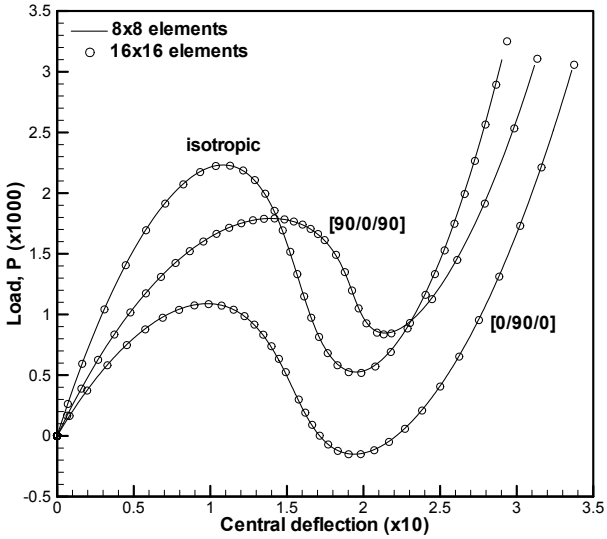

Figure 9b: Load-deflection curves of the 12.7 unit thick hinged cylindrical roof.

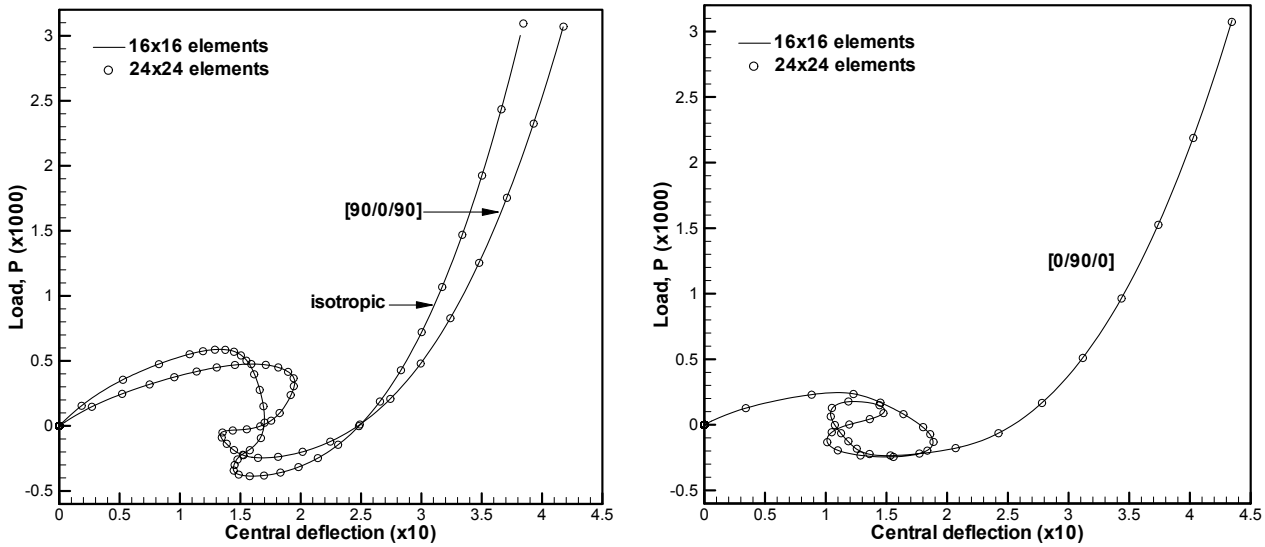

Figure 9c: Load-deflection curves of the 6.35 unit thick hinged cylindrical roof.